Small and large cutaneous fibers display different excitability properties to slowly increasing ramp pulses

Tigerholm, Jenny; Hoberg, Tatiana Nielson; Brønnum, Dorthe; Vittinghus, Mette; Frahm, Ken Steffen; Mørch, Carsten Dahl

Published in:
Journal of Neurophysiology

DOI (link to publication from Publisher):
10.1152/jn.00629.2019

Publication date:
2020

Document Version
Accepted author manuscript, peer reviewed version

Title: Small and large cutaneous fibers display different excitability properties to slowly increasing ramp pulses - assessed with the perception threshold tracking technique

Authors: Jenny Tigerholm[2,], Tatiana Nielson Hoberg,[1], Dorthe Brønnum[1,3], Mette Vittinghus[1,4], Ken Steffen Frahm[1,2], Carsten Dahl Mørch[1,2*].

(1) SMI, Department of Health Science and Technology, Aalborg University, Fredrik Bajers Vej 7 D3, 9220 Aalborg, Denmark.

(2) Integrative Neurodcience group, CNAP – Center for Neuroplasticity and Pain, SMI, Department of Health Science and Technology, Aalborg University, Fredrik Bajers Vej 7 D3, 9220 Aalborg, Denmark.

(3) Centre for Clinical Research, North Denmark Regional Hospital, Bispensgade 37, 9800, Hjørring, Denmark

(4) It-center for Telemedicin, Region Midtjylland, Oluf Palmes Allé 36, 8200 Aarhus N, Denmark

Acknowledgements

Funded by Center for Neuroplasticity and Pain (CNAP). CNAP is supported by the Danish National Research Foundation (DNRF121).

*Corresponding Author:

Carsten Dahl Mørch,

Integrative Neuroscience group, CNAP

25 Department of Health Science and Technology,

26 Fredrik Bajers Vej 7

27 9220 Aalborg Ø, Denmark;

28 Phone: (+45) 9940 8757

29 Mail: cdahl@hst.aau.dk

30

31 Running title: Accommodation in cutaneous nerves

Abstract

The excitability of large nerve fibers is reduced when their membrane potential is slowly depolarizing, i.e. the fibers display accommodation. The aim of this study was to assess accommodation in small (mainly Aδ) and large (Aβ) cutaneous sensory nerve fibers using the perception threshold tracking (PTT) technique.

Linearly increasing ramp currents (1 ms -200 ms) were used to assess the excitability of the nerve fibers by cutaneous electrical stimulation. To investigate the PPT technique's ability to preferentially activate different fiber types, topical application of lidocaine/prilocaine (EMLA) or a placebo cream was applied. By means of computational modelling, the underlying mechanisms governing the perception threshold in the two fiber types was studied. The axon models included the voltage-gated ion channels: Na_{TTXs}, Na_{TTXr}, Na_P, K_{Dr}, K_M, and HCN.

Large fibers displayed accommodation, whereas small fibers did not display accommodation ($p<0.05$). For the pin electrode, a significant interaction was observed between cream (EMLA or placebo) and pulse duration ($p<0.05$) whereas for the patch electrode, there was no significant interaction between cream and duration which supports the pin electrode's preferential activation of small fibers. The results from the computational model suggested that

differences in accommodation between the two fiber types may originate from selective expression of voltage-gated ion channels, particularly the transient Na_{TTXr} and/or K_{Dr}.

55 The PTT technique could assess the excitability changes during accommodation in different
56 nerve fibers. Therefore, the PTT technique may be a useful tool for studying excitability in
57 nerve fibers both in healthy as well as in pathological conditions.
58
59 Keywords: Accommodation, perception threshold tracking technique, nerve fiber excitability,
60 voltage-gated ion channels, multi-compartmental model

New & Noteworthy

When large nerve fibers are stimulated by long, slowly increasing electrical pulses interactive mechanisms counteract the stimulation, which is called accommodation. The perception threshold tracking technique was able to assess accommodation in both small and large fibers. The novelty of this study is that large fibers displayed accommodation, whereas small fibers did not. Additionally, the difference in accommodation between the fiber could be linked to expression of voltage-gated ion channels by means of computational modeling.

Introduction

Neuropathic pain has a prevalence rate of 6.9 % - 10 % (van Hecke, et al., 2014) and manifests itself through symptoms of burning pain, shooting pain, allodynia, and hyperesthesia (Hovaguimian & Gibbons, 2011). The underlying mechanisms of small fiber neuropathy are unknown, but altered excitability has been detected both in patients with peripheral neuropathic pain as well as in animal models of neuropathy (Serra, et al., 2012; Serra, et al., 2011). Tactile information is passed through afferents with larger diameters (Aβ fibers), whereas nociceptive information is passed through small diameter afferent fibers (C and Aδ fibers). The main obstacle when studying small fibers in humans is their high electrical activation thresholds which makes it technically challenging to study the fibers in isolation without activation of the large fibers. To overcome this obstacle, electrodes with small cathodes (pin electrodes) have been used (Bromm & Meier, 1984; Nilsson & Schouenborg, 1999; Kaube, et al., 2000; Inui, et al., 2002; Klein, et al., 2004; Otsuru, et al., 2009; Lelic, et al., 2012; Hennings , et al., 2017). These Pin electrodes preferentially activate the superficial small fibers by generating a high current density in epidermis and thereby avoiding activating the large fibers which are terminating in dermis (Hilliges, et al., 1995; Ebenezer, et al., 2007 ; Provitera, et al., 2007; Mørch C, et al., 2011; Myers, et al., 2013). Estimations of nerve fiber conductance velocity support the non-invasive pin electrode's preferential activation of small fibers (Inui, et al., 2002; Otsuru, et al., 2009; Lelic, et al., 2012). Test subjects perceive the pin electrode stimulation as needle pricking, stabbing and sharp, and distinctly different from large cathode electrodes (patch electrodes) designed to activate large fibers (Bromm & Meier, 1984; Hugosdottir, et al., 2017; Lelic, et al., 2012). At low stimulation intensities, non-invasive pin electrodes preferentially activate the thinly

95 myelinated small Aδ fibers (Inui, et al., 2002; Lelic, et al., 2012), whereas the invasive pin
96 electrode may also activate the unmyelinated C fibers (Otsuru, et al., 2009).
97
98 Our research group has developed the Perception Threshold Tracking (PTT) technique,
99 which assesses neuronal excitability by measuring the perception threshold to cutaneous
100 electrical stimulation, using different pulse shapes and durations (Hennings , et al., 2017;
101 Hugosdottir, et al., 2017). The perception threshold is defined, in the current study, as the
102 intensity of the stimulus required for the subject to perceive the stimulus at the site of
103 stimulation. In a recent study, the strength-duration properties and threshold electrotonus
104 were assessed for both small and large fibers (Hennings , et al., 2017). Interestingly, the
105 excitability assessments differed between small and large fibers indicating different
106 membrane properties between the two fiber types. In this study, the objective was to study the
107 excitability to linearly increasing cutaneous ramp stimulation in small and large fibers. For
108 motor fibers, the excitability of both small and large diameter motor neurons has been shown
109 to be reduced for long ramp pre-pulses (Hennings, et al., 2005). When large nerve fibers are
110 stimulated by long, slowly increasing electrical stimulation (50-200 ms) a higher stimulation
111 current is needed to activate the fiber compared to a shorter electrical stimulation (Lucas,
112 1907; Kugelberg, 1944) (see figure 1A). This altered excitability will in the current study be
113 referred to as fiber accommodation (Kugelberg, 1944). The ability of accommodation of
114 each nerve fiber is determined by the intrinsic properties of its membrane (Stoney S &
115 Machne, 1969). Particularly, the resting membrane potential has been shown to modulate the
116 accommodation in large fibers (Baker & Bostock, 1989 ; Bostock, et al., 1991). The strong
117 influence of the resting membrane potential on accommodation indicates that voltage-gated
118 ion channels play a significant role in generating accommodation. From patch clamp and
119 threshold electrotonus experiments in rats, potassium channels have been identified to alter
120 the accommodation by rectification of the membrane potential (Baker & Bostock, 1989 ;

Stoney S & Machne, 1969). However, a computational study has shown that almost any alteration of the density of the voltage-gated ion channel will alter the accommodation, whereby the parameter which had the strongest influence was the inactivation of transient sodium channels (Frankenhaeuser & Vallbo, 1965). Since small and large fibers have different expressions of voltage-gated ion channels (Akopian, et al., 1996; Gold, et al., 1996; Djouhri, et al., 2003; Gao , et al., 2012), the hypothesis is that their respective accommodations may differ. For instance, small fibers express two TTX resistant sodium channels ($Na_v1.8$ and $Na_v1.9$), which are lacking in large fibers (Akopian, et al., 1996; Djouhri, et al., 2003). Therefore, the purpose of this study was to measure the accommodation in small fibers as well as large fibers, and link the accommodation to membrane properties.

Materials and methods

This is a combined clinical and computational study (see figure 1). In the experimental study, the accommodation in small and large cutaneous nerve fibers was assessed using the PTT technique. For long ramp pulses (>20 ms) the excitability can be reduced, and the intensity needed for the subject to perceive the stimulus is increased, this is denoted as accommodation in the current study. Topical application of EMLA cream was used to validate the pin electrode's preferential activation of small fibers. To identify the possible mechanisms for the different accommodation between the two fiber classes, two multi-compartment models were developed.

Experimental study

Subjects

20 healthy subjects participated in the study, however one subject was excluded due to technical issues, thus data analysis was completed for 19 subjects (10 males, 9 females, age 34.6±13.3 years). The subjects were given detailed written and verbal information and signed an informed consent form prior to participation. The study was approved by the local ethics committee (Den Videnskabsetiske Komité, Region Nordjylland, approval number: N-20120046) and conducted according to the declaration of Helsinki. Exclusion criteria were; a) addiction or prior addiction to cannabis, opioids, or other drugs, b) skin diseases, c) infectious diseases, d) conditions that might lead to peripheral neuropathy, and e) pain relieving medication within the last 48 hours.

159

160 **Experimental setup**

161

162 The experiment consisted of one experimental session lasting 3.5 hours. The subjects were
163 placed in a comfortable inclined position in a hospital bed throughout the session.

164

165 Two surface electrodes were used to preferentially activate small and large fibers as
166 described in previous papers (Hennings , et al., 2017). A cutaneous pin electrode with a
167 circular array of 16 small area cathodes made of blunted stainless steel with a diameter of 0.2
168 mm protruding 1 mm from the base of the electrode and a concentric stainless steel disc
169 anode with an area of 8.8 mm was used to preferentially activate small fibers (see figure 1B).
170 A large area surface AgAgCl cathode (Patch, 20 x 15 mm; Neuroline 700; Ambu A/S,
171 Ballerup, Denmark) in combination with a larger anode (5 x 9 cm; Pals Neurostimulation
172 Electrode Axelgaard, CO., Ltd., California) was used to preferentially activate large fibers.

173

174 PTT was performed with a computer-controlled program, LabBench (SMI®, Aalborg
175 University, Denmark) stimulating with a DS5 Isolated Bipolar Current Stimulator (Digitimer
176 Ltd, Letchworth Garden City, UK). Perception thresholds were assessed by an adaptive
177 staircase method; Stimuli were given with an inter-stimulus interval of 1 second and
178 increased by 15% of the last stimulus until the subject indicated perception by pressing a
179 handheld response button (SMI®, Aalborg University, Denmark). After indicating perception
180 by pushing the button, the stimulation intensity was maintained two consecutive times and if
181 these stimulations were also perceived, the intensity was decreased by 15% until the
182 stimulation was not perceived anymore, as indicated by not responding three consecutive
183 times. In the four following sequences the intensity increased and decreased by 7.5%, 3.5%,

3%, and 3%. The perception threshold was calculated as a weighted average of all 10 measurements. Accommodation was assessed by linearly increasing ramp currents of 1 ms, 10 ms, 25 ms, 50 ms, 100 ms and 200 ms. The order of the electrical stimulations was randomized in a single-blinded manner.

To validate that the pin electrode preferentially activates the small fibers, topical application of EMLA was used to block the small fibers (which should cause increase activation threshold) (Bjerring & Arendt-Nielsen, 1990). A cream similar in color, smell, and consistency was used as placebo. The creams were supplied in identical vials and the order of the creams (EMLA or placebo) was randomized 1:1. The experimenter applied 4 grams of cream (either EMLA or placebo) to a 5 x 5 cm skin area on the volar part of the forearm 5 cm distal from elbow pit under an impermeable plastic occlusive film. After 60 minutes the cream was removed from the first arm and a cream was applied similarly to the opposite forearm. Testing began on each arm 30 minutes after removal of the cream to ensure a stable effect of EMLA during performance of the perception threshold measurements.

Data analysis

All statistical calculations were performed using MATLAB 2016b (MathWorks, Natick, Massachusetts, USA) and SPSS 25 (IBM SPSS Statistics, Armonk, New York, USA). To obtain normality, the perception thresholds were normalized to the threshold for the 1 ms duration pulse and log transformed. A three-way repeated measures ANOVA was carried out to analyze the difference between the electrodes (pin or patch), the cream (EMLA and placebo) and the ramp pulse durations (1 ms, 10 ms, 25 ms, 50 ms, 100 ms and 200 ms). In

209 the event of significant interactions involving the electrodes, a two-way repeated measures
210 ANOVA was carried out for each electrode with cream (EMLA and placebo) and ramp pulse
211 durations (1 ms, 10 ms, 25 ms, 50 ms, 100 ms and 200 ms). The Greenhouse-Geisser method
212 was used to adjust for non-spherical covariance matrices. Pairwise comparisons of the
213 estimated marginal means were corrected for multiple-comparison with the Sidak method
214 when comparing differences between ramp pulse durations. Statistical significance was
215 defined as $p < 0.05$.
216

217 Computational model

218

219 Two computational fiber models were developed in the simulator environment NEURON (
220 (Hines & Carnevale, 1997), version 7.6); one myelinated fiber model (Aβ model)
221 representing a large fiber and one unmyelinated fiber model representing the unmyelinated
222 intraepidermal part of an Aδ fiber (Aδ model). The cutaneous electrical stimulation will
223 activate a population of fibers, but in order to reduce the computational complexity, one fiber
224 will represent the mean of a population of fibers. No sensory transductions were modeled,
225 because during electrical stimulation an action potential is generated by shifting the voltage
226 across the cell membrane and no sensory transduction within the sensory terminal is
227 occurring. Instead of a sensory terminal, the Aβ model terminated in a node of Ranvier. All
228 morphological parameters are listed in table 1. The number of compartments were 5000 for
229 the Aδ model and 5133 for the Aβ model (node of Ranvier = 3 compartments, internode =
230 500 compartments and Juxtaparanode= 5 compartments) and the equations were solved using
231 the variable time step method in NEURON. The resting membrane potential was set to -60
232 mV (Fang, et al., 2005). The delayed rectifier potassium channels' voltage dependency was
233 shifted 15 mV towards hyperpolarization in order to generate a rectification of the action

potential. Four sodium channels were implemented: two transient TTX- sensitive sodium currents (Na_{TTXs}), the transient TTX resistant sodium current (Na_{TTXr}) and the persistent sodium current (Na_P).

The morphological parameters are listed in table 1.

Table 1. Parameters of the morphology for the fiber models

	Aδ model	**Aβ model**	**Reference**
Diameter	0.5-3.5 µm	9 µm	
Nodal length		3 µm	(Berthold & Rydmark, 1983)
Internodal length		500 µm	(Nilsson & Berthold. , 1988; Provitera, et al., 2007)
Juxtaparanodal length		5 µm	(Poliak, et al., 2003)
Capacitance nodal/branch		1 µF/cm^2	(Amir & Devor, 2003)
Capacitance myelin		0.0141 µF/cm^2	(Amir & Devor, 2003) C=1/(myelin sheet +1)
Resting membrane potential	-60 mV	-60 mV	(Fang, et al., 2005)
Number of myelin sheets		70	(Provitera, et al., 2007; Berthold & Rydmark, 1983)
Intra cellular resistance	130 Ωcm	130 Ωcm	
Total model length	5000 µm	5133 µm	

242

243

244 *Table 2. The models of voltage-gated ion channels. K_{Dr}: delayed rectifier potassium channel,*

245 *K_M: slow potassium channel, HCN: hyperpolarization-activated current, Na_{TTXs}: TTX*

246 *sensitive current, Na_{TTXr}: TTX resistant current, Na_P: persistent sodium current.*

247

248

Aδ model	**Model Reference**	**Spatial location**	**Maximal Conductance (S/cm^2)**
Na_{TTXr} (Na_v 1.8)	(Tigerholm, et al., 2014)	Unmyelinated nerve	0.0435
Na_p (Na_v 1.9)	(Tigerholm, et al., 2014)	Unmyelinated nerve	$3.5549x10^{-5}$
Na_{TTXs} (mainly Na_v 1.7)	(Tigerholm, et al., 2014)	Unmyelinated nerve	0.0166
K_{Dr}	(Tigerholm, et al., 2014)	Unmyelinated nerve	$3.4023x10^{-4}$
K_M	(Tigerholm, et al., 2014)	Unmyelinated nerve	$1.0460x10^{-6}$
HCN	(Tigerholm, et al., 2014)	Unmyelinated nerve	$1.4275x10^{-6}$
Aβ model			
Na_{TTXs} (Na_v 1.6)	(Watanabe, et al., 2002)	Nodes of Ranvier	0.4394
Na_p	(Jankelowitz, et al., 2007)	Nodes of Ranvier	$7.7731x10^{-5}$
K_{Dr}	(Tigerholm, et al., 2014)	Juxtaparanode	0.0065
HCN	(Tigerholm, et al., 2014)	Juxtaparanode	$9.1358x10^{-4}$
K_M	(Tigerholm, et al., 2014)	Nodes of Ranvier	0.0021
Leak channel	(Tigerholm, et al., 2014)	Internode	$1.0000x10^{-7}$

Table 3. Action potential characteristics

	Aδ model	**Aβ model**

Action potential height	Initiation: 123 ms End of the model: 120 ms	Initiation: 127 ms End of the model:114 ms
Action potential width	Initiation: 3.7 ms End of the model: 3.6 ms	Initiation: 1.6 ms End of the model: 1.5 ms
Velocity	0.54m/s	11m/s

Aδ model

The Aδ model was developed by modifying a previously published, detailed multi-compartment model of a C-fiber (Tigerholm, et al., 2014; Tigerholm, et al., 2015). In this study, the C-fiber model has been simplified by the removal of the ion concentration dynamics. The diameter was increased for the C-fiber model to be consistent with an Aδ-fiber's morphology. The Aδ model consists of two sections. The first section (500 μm) starts with a diameter of 0.5 μm, which is increased linearly to 3.5 μm in diameter. The second section is a cylinder with a diameter of 3.5 μm connecting to the first section (see figure 1C). The Aδ-model did not include any myelination since only the superficial part of the Aδ fiber was modeled, and the Aδ fibers lose their myelin when entering the epidermis (Provitera, et al., 2007). One TTX-sensitive sodium channel (Na_{TTXs}, mainly Na_v 1.7) and two resistant sodium channels were implemented (Na_v 1.8 and Na_v 1.9). Additionally, two potassium channels and one HCN channel were implemented. See table 2 for the voltage-gated ion channel model references for the equations of the steady-state parameters, and their time-constants. The equations describing the ion channel dynamics are stated in the supplemental data. The action potential characteristics are presented in table 3.

Aβ model

The Aβ model consists of three different morphological sections: nodes of Ranvier, Juxtaparanode and myelinated fiber (see figure 1C). The three different sections of the membrane have different electrical properties as well as distribution of voltage-gated ion channels (see table 1 and 2). The capacitance of the myelin section of the axon is dependent of the thickness of the myelin i.e. the number of myelin sheets (Amir & Devor, 2003). The capacitance in the current study was calculated by C=1/(the number of myelin sheets +1), which is a method adopted from the Amir and Devor study (2003) . One TTX-sensitive sodium channel (Na_{TTXs}, Nav 1.6) and one persistent sodium channel (Na_P) were implemented. Additionally, the two potassium channels and the HCN channel which were implemented in the Aδ model was also implemented in the large fiber model. See tabl e 2 for the voltage-gated channel model references for the equations of the steady-state parameters and their time-constants. The equations describing the ion channel dynamics are stated in the supplemental data. https://doi.org/10.5281/zenodo.3975475. The action potential characteristics are presented in table 3. The internodal distance is set to 500 μm, which is one quarter of the internodal distance measured in deeper layers (Nilsson & Berthold., 1988) since the internodal length of the nerve fibers is reduced when they enter superficial layers of the skin (Provitera, et al., 2007).

Extracellular stimulation

To simulate the cutaneous stimulation, the extracellular potential at the most superficial section of the fiber models was changed with the same shape as the current pulse applied

through the electrode in the experiment. For the Aδ model, the extracellular potential was altered for a section of 500 μm through the built-in function of the extracellular in NEURON. For the Aβ fiber model, the extracellular potential of the first node of Ranvier was altered. The shape of the extracellular alteration was a ramp pulse with the same durations as were tested in the experimental study. The extracellular potential was increased until the fiber model generated an action potential (membrane potential higher than 0 mV) which propagates to the end of the fiber model.

Constraints of the computational models

The maximum conductances of the voltage-gated ion channels were defined by the following constraints:

1) For increasing durations of the ramp simulation, in the interval 50 ms - 200 ms, the activation threshold of the Aδ model should be declining or constant.
2) For increasing durations of the extracellular potential in the interval 50 ms - 200 ms, the activation threshold should increase for the Aβ model.
3) If an action potential is generated (membrane potential > 0 mV), it should propagate to the end of the nerve fiber model
4) The Na_{TTXr} current should generate the action potential in the Aδ model (Blair & Bean, 2002)
5) The action potential should be higher than 0 mV at the last section of the model for the simulation to be classified as a successful propagation.
6) The HCN maximum conductance should be at least two times higher in the Aβ model than in the Aδ model (Gao , et al., 2012)

Results

Small and large fibers have different accommodation to ramp pulse electrical stimulation

The absolute value of the perception threshold was higher for the patch electrode than the pin electrode across all durations of the ramp stimulations (figure 2). This was a direct consequence of the different cathode configurations. More interestingly, a significant difference of log-transformed and normalized thresholds was observed between the electrodes ($p < 0.05$) and interactions between cream (EMLA and placebo) and electrodes ($p < 0.01$) as well as between electrode and pulse duration ($p < 0.001$) indicating that accommodation was different between the two electrodes (see figure 2C). The electrodes were therefore analyzed individually.

For the patch electrode, significantly different thresholds were observed between the pulse durations ($p < 0.001$), but not between cream ($p = 0.06$), and there was no interaction between cream and duration. Comparing the estimated marginal means of the pulse durations showed that the thresholds for the 1 ms, 100 ms and the 200 ms pulses were higher than the thresholds to 20 ms, 50 ms pulses ($p < 0.05$; figure 2C), indicating that large nerve fibers accommodated to long duration ramp pulses.

For stimulation with the pin electrode in the EMLA arm, the 1 ms pulse threshold was significantly higher than the threshold to the 50 ms pulse ($p < 0.05$). No other significant threshold differences were observed between the 1 ms pulse and any of the other pulse durations, indicating similar, though not as pronounced, accommodation as large nerve fibers

activated by the patch electrode. Thus, the nerve fibers activated under this condition are probable not only large fibers, but a combination of both small and large fibers.

For stimulation with the pin electrode in the placebo arm, the 1 ms pulse threshold were significantly higher than all the longer pulses ($p<0.05$), indicating the small fibers activated by the pin electrode did not accommodate to ramp pulses.

The accommodation generated in the computational model

A wide range of voltage-gated ion channels with different dynamic properties were implemented in the computational model. In figure 3, the ionic currents during an action potential is illustrated. In figure 4A, the extracellular potential alteration needed to generate an action potential for different duration of the ramp pulses is illustrated. For a 1 ms pulse duration, the increase of the extracellular potential needed to activate the Aδ model was 4.3 times larger than the Aβ model. This is consistent with the high electrical stimulation intensity needed to activate small fibers with the patch electrode. In figure 4B, the relative extracellular potential alteration needed to generate an action potential is illustrated. The excitability of the two nerve fiber models was affected differently by long ramp pulses (see figure 4 C-F). For the Aδ model, the membrane became more excitable when the membrane potential was increasing slowly (see figure 4C and 4E). For the 200 ms slowly-increasing stimulation the small fiber model even starts to produce two spikes at the end of the stimulation. For the Aβ model, slow depolarization leads to reduced excitability and the inability to generate an action potential when the membrane is too depolarized (see figure 4D and 4F).

375

376 **The influence of voltage-gated ion channels on accommodation**

377

378 The influence of subtypes of voltage-gated ion channels on the accommodation is illustrated
379 in figure 5. For the Aβ fiber model, an alteration of the Na_{TTXs} channel had the strongest
380 influence on the accommodation, which can be explained by the high channel density in the
381 node of Ranvier. However, changing any of the ion channel densities influenced the
382 accommodation curve in the Aβ model. For the Aδ model, changing the maximum
383 conductance of subtypes of ion channels did not alter the accommodation substantially.
384 Furthermore, when both the potassium channels' conductances were reduced with 50%, the
385 Aβ model did not display any accommodation (see figure 5B, green dotted line). The purpose
386 of this simulation was to evaluate the consistency between the behavior of the computational
387 model and the experimental results, showing no accommodation when the potassium
388 channels were blocked in an animal study (Stoney S & Machne, 1969).

389

390 To further analyze the influence of voltage-gated ion channels, larger perturbation of the
391 maximum conductance was implemented in the computational model (see figure 6). When
392 the maximum delayed rectifier conductance was reduced by 60%, the Aβ model did not
393 display any accommodation (see figure 6A-B, blue line). If instead the maximum
394 conductance of delayed rectifier potassium was increased by 300% in the Aδ model, the
395 model displayed accommodation in a similar fashion as the Aβ model (see figure 6C-D, blue
396 dashed line). If instead the slow dynamic voltage-gated ion channels (HCN, Na_P, and K_M)
397 were removed from the nerve fiber models, the accommodation was marginally altered (see
398 figure 6, green lines). Interestingly, if all voltage-gated ion channels except the Na_{TTXs}

channel were removed from the Aβ model, the model could still generate accommodation (see figure 6, light blue lines).

The influence of inactivation of sodium on accommodation

The inactivation of the transient sodium channels for the two models are compared in figure 7 where the extracellular potential was altered up to 10 mV and with a duration of 200 ms ramp pulse. The Na_{TTXs} channels in the Aβ model were 84 % inactivated while the Na_{TTXr} channels in the Aδ model were only 65% inactivated (see figure 7B). Despite that 10 mV alteration of the extracellular potential depolarizes the Aβ model less than the Aδ model (see figure 7A).

To further study, the influence of inactivation of sodium on accommodation, the steady-state inactivation curves of either Na_{TTXs} (Aβ model) or the Na_{TTXr} (Aδ model) were shifted. To compensate for the general excitability, the maximum conductance of the Na_{TTXs} was increased (Aβ model), or the Na_{TTXr} was adjusted (Aδ model), whereby the activation threshold for the 1 ms ramp stimulation remained within 5 % compared to the control model (no shifts of the inactivation). By shifting the steady-state inactivation curves, the accommodation could be generated in the Aδ model (dashed lines, Figure 7E-F) and removed in the Aβ model (dashed lines, Figure 7C-D).

Discussion

In this study, accommodation in small and large sensory fibers was estimated by the PTT technique. The PPT experiment showed that large fibers displayed accommodation to long ramp stimulation pulses, while small fibers did not. Furthermore, the results from the computational model suggested that the selective expression of voltage-gated ion channels may account for the difference in accommodation between the two fiber types.

Accommodation to ramp electrical stimulations differed between small and large fibers

Accommodation of nerve fibers has mainly been studied in humans by assessing the compound action potential in large fibers (Baker & Bostock, 1989 ; Bostock, et al., 1998; Kiernan , et al., 2000). Assessment of the compound action potential can be performed on large fibers but this is technically challenging to detect in small fibers. Therefore, our research group has previously used the perception threshold instead of compounded action potential for studying the strength-duration relationship and the threshold electrotonus (Hennings , et al., 2017; Hugosdottir, et al., 2017). In this study, accommodation has been studied in small and large fibers with this PTT technique. Accommodation of the median

nerve has previously been estimated by assessing the motor compound action potential (Hennings, et al., 2005). The threshold of the median nerve for 200 ms was 88%-96% of the threshold for the 1 ms duration. In our study, the threshold of the large fibers for 200 ms was 61% of the threshold of 1 ms duration. The lower value measured in our study could be explained by the difference in fiber types, motor vs sensory fibers. This is supported by the classic work of Kugelberg showing that motor fibers have more pronounced accommodation properties than the sensory fibers (Kugelberg, 1944). Interestingly, small fibers did not display accommodation i.e. had no significant increase in perception threshold for long ramp simulation. In our previous study, threshold electrotonus was studied for both large and small sensory fibers, and the result showed no significant differences between the perception thresholds of the two fiber types except for long (80ms) hyperpolarizing prepulses (Hennings , et al., 2017). The threshold electrotonus protocol assesses the effect of altering the membrane potential of nerve fibers activation, which is another method for probing accommodation. The discrepancy between the current study and our previous study could be explained by the fact that only a small prepulse was used.

Moreover, the ability of accommodation in nerve fibers is essential as it attempts to counteract the effect of a sustained stimulus, thereby limiting the generation of action potentials and repetitive firing from the neurons (Baker & Bostock, 1989). In the computational model of small fibers, multiple spikes were generated when a 200 ms ramp stimulation was applied (see figure 4C). Human and animal models of neuropathic pain states showed spontaneous activity or duplets when small fibers were stimulated (Serra, et al., 2012; Serra, et al., 2011). A possible explanation for this could be that the increased excitability occurring in these pain states leads to a depolarized membrane and thereby an enhanced possibility of multiple spike generation in the small fibers.

Different expression of voltage-gated ion channels may generate the difference in accommodation between the two fiber types.

The underlying mechanisms of accommodation have been studied in both threshold tracking experiments, DRG patch clamp experiments as well as in computational models (Baker & Bostock, 1989 ; Stoney S & Machne, 1969; Frankenhaeuser & Vallbo, 1965; Hennings, et al., 2005). It is clear that voltage-gated ion channels play an important role in generating the accommodation since altering the membrane potential or blocking potassium channels has a strong influence on accommodation (Bostock, et al., 1991; Baker & Bostock, 1989 ; Baker M, et al., 1987). However, which subtypes of the voltage-gated ion channels have the most substantial influence on the accommodation is still unclear. The ion channel parameter which had the most substantial influence on accommodation in a computational study was the inactivation of the sodium channel (Frankenhaeuser & Vallbo, 1965). However, almost all ion channel parameters altered in the computational model had a strong influence on the accommodation (Frankenhaeuser & Vallbo, 1965). This may explain why blocked potassium channels lead to almost a complete loss of accommodation in a threshold electrotonus experiment in rats (Baker & Bostock, 1989). This behavior could be reproduced in our Aβ fiber model when the maximum conductance of the potassium channels was reduced by 50% (see figure 5D). One of the most interesting studies of accommodation is a patch clamp study in which the excitability to an intracellular current stimulation in large DRG somas is studied (Stoney S & Machne, 1969). In that study, the membrane potential plateaued for a long ramp current stimulation and the action potential was not generated at the end of the stimulation but instead in the middle of the stimulation. This is consistent with the behavior displayed by

495 the computational model of the Aβ fiber where the action potential was generated at 80 ms
496 for a ramp pulse of 200 ms (see figure 4D and 4F).
497
498 Furthermore, a support for the sodium inactivation important contribution to accommodation
499 is the result that accommodation could be generated in the computational model when only
500 TTX-sensitive sodium channel was implemented in the Aβ model (see figure 6B). These
501 results suggest that the difference in inactivation between the Na_{TTXr} and Na_{TTXs} channels
502 may contribute to generate the difference in accommodation measured between small and
503 large fibers. The Na_{TTXr} sodium channel (Na_v 1.8) is only expressed in small fibers (Djouhri,
504 et al., 2003) and the channel is inactivated at more depolarized membrane potential
505 (Inactivation $V_{1/2}$ =-32 mV (Blair & Bean, 2002)) than the Na_{TTXs} sodium channel (Na_v1.6),
506 which is expressed in large fibers (Inactivation $V_{1/2}$ =-55 mV (Smith, et al., 1998; Caldwell,
507 et al., 2000)).
508
509
510
511 **Clinical implications for perception threshold tracking**
512
513 Available diagnostic tools to determine small fiber functionality mainly include clinical
514 examination, skin biopsies and quantitative sensory testing. Such available diagnostic tools
515 for small fiber neuropathy are insufficient to explore the mechanisms underlying neuropathy
516 and there is a need for new methods (Smith, et al., 2017). Compared to the existing method
517 for probing excitability in small fibers (microneurography) the PTT technique is an
518 inexpensive and non-invasive method which makes it suitable for clinical settings. Whereas
519 the PPT technique is a newly developed method and the diagnostic accuracy of PPT

techniques has not been evaluated, this study, as well as our previous studies (Hennings , et al., 2017; Hugosdottir, et al., 2017), have shown that the PTT technique may potentially be able to distinguish between membrane properties of both small and large nerve fibers. Further development of both the PPT method and the fundamental understanding of membrane currents related to neuropathy is required, but the PTT technique certainly has the possibility to become a diagnostic tool for neuropathy.

Limitations

The PTT technique indirectly measures the membrane excitability in a similar way as established methods of threshold tracking of the compound action potential. The main disadvantages with the perception threshold assessment are the influence of the central nervous system. To reduce the influence of the central nervous system a low frequency as well as low intensity stimulation are used during PTT since high frequencies and high intensities are prone to induce plasticity changes in the central nervous system (Klein, et al., 2004; Xia, et al., 2016). The variability between different subjects is of course substantial, but has been controlled for when using the data to fit the computational model by normalizing the data of the individual participants. The major cause of between subject variation in healthy participants is probably the distance from the cathode to the nerve fiber ending. Therefore, skin thickness and electrode placement may contribute most to the between subject variation. A major source of within subject variation is habituation which will cause the perception threshold to increase during the experiment. To reduce this effect, in the current study, the different durations of the ramp pulse were delivered in a randomized order.

One of the limitations of the computational model is that it did not include any calcium channels which play an important role in regulating the excitability changes in nerve fibers. Finally, the model did not include the influence of the electrical properties of the skin, but assumed that this would not affect the activation of the nerve fibers. This is a simplification as the capacitive properties of the tissue will smoothen the electrical field and thus the electrical field at the nerve fibers will not be exactly the same as seen on the skin surface. An additional limitation of the computational model is the number of unknown parameters, particularly the maximum conductance of the voltage-gated ion channels.

Author Contributions

Conceptualization of the study was done by JT, TNH, KSF and CDM. All experimental data were collected and analyzed by TNH, DB, MV, and CDM. The computational work was performed by JT. The manuscript draft was written by JT and TNH. All authors revised the manuscript and approved the final version for publication.

Acknowledgement

Center for Neuroplasticity and Pain (CNAP) is supported by the Danish National Research Foundation (DNRF121). A special thanks to Laila Adela Zadeh Nielsen and Ditte-Maj Kudahl Nielsen for helping collect the experimental data.

Reference

Akopian A, Sivilotti L, Wood JN, A tetrodotoxin-resistant voltage-gated sodium channel expressed by sensory neurons. *Nature*, 379:257–262, 1996

Amir R, Devor M, Electrical excitability of the soma of sensory neurons is required for spike invasion of the soma, but not for through-conduction. *Biophys J*, 84:2181-2191, 2003

Baker M, M., Bostock H, H. & Martius, P., 1987 . Function and distribution of three types of rectifying channel in rat spinal root myelinated axons.. *J Physiol.,* Volume 383, pp. 45-67.

Baker M, Bostock H, Depolarization changes the mechanism of accommodation in rat and human motor axons. *J Physiol*, 411:545-6, 1989.

Berthold CH, Rydmark M, Electron microscopic serial section analysis of nodes of Ranvier in lumbar spinal roots of the cat: A morphometric study of nodal compartments in fibres of different sizes. *Journal of Neurocytology*, 12:537–565, 1983.

Bjerring P, Arendt-Nielsen L, Depth and duration of skin analgesia to needle insertion after topical application of EMLA cream, *Br J Anaesth*., 64:173-177, 1990

Blair N, Bean BP, Roles of tetrodotoxin (TTX)-sensitive Na+ current, TTX-resistant Na+ current, and Ca2+ current in the action potentials of nociceptive sensory neurons. *J Neurosci,* 22:10277-90, 2002.

Bostock H, Baker M, Grafe P, Reid G, Changes in excitability and accommodation of human motor axons following brief periods of ischaemia, *J Physiol.,* 441:513-535, 1991.

Bostock, H., Cikurel, K. & Burke, D., 1998. Threshold tracking techniques in the study of human peripheral nerve. *Muscle & Nerve*, 21:137–158.

Bromm B, Meier WT, The intracutaneous stimulus – a new pain model for algesimetric studies. *Methods Find Exp Clin Pharmacol*, 6:405–410, 1984.

Caldwell JH, Schaller KL, Lasher RS, Peles E, Levinson SR, Sodium channel Nav1. 6 is localized at nodes of ranvier, dendrites, and synapses. *Proc Natl Acad Sci U S A.*, 97:5616–5620, 2000.

Djouhri L, Fang X, Okuse K, Wood JN, Berry CM, Lawson SN. The TTX-resistant sodium channel Nav1.8 (SNS/PN3): expression and correlation with membrane properties in rat nociceptive primary afferent neurons, *J Physiol.,* 550:739-52, 2003.

Ebenezer GJ1, McArthur JC, Thomas D, Murinson B, Hauer P, Polydefkis M, Griffin JW, Denervation of skin in neuropathies: the sequence of axonal and Schwann cell changes in skin biopsies. *Brain,* 130:2703-2714, 2007.

Fang X, McMullan S, Lawson S, Djouhri L, Electrophysiological differences between nociceptive and non-nociceptive dorsal root ganglion neurones in the rat in vivo. *J Physiol*, 565:927–943, 2005.

616 **Frankenhaeuser B, Vallbo ÅB**, Accommodation in myelinated nerve fibres of Xenopus
617 laevis as computed on the basis of voltage clamp data. *Acta physiologica Scandinavica*, 63:1-
618 20, 1965.
619
620 **Gao LL, McMullan S, Djouhri L, Acosta C, Harper AA, Lawson SN,** Expression and
621 properties of hyperpolarization-activated current in rat dorsal root ganglion neurons with
622 known sensory function. *PLoS One*, 7, 2012.
623
624 **Gold MS, Shuster MJ, Levine JD,** Characterization of six voltage-gated K+ currents in
625 adult rat sensory neurons, *J Neurophysiol*., 75:2629-46, 1996.
626
627 **Hennings K, Frahm KS, Petrini, L, Andersen OK, Arendt-Nielsen L, Mørch CD,**
628 Membrane properties in small cutaneous nerve fibers in humans. *Muscle & Nerve*, 2:.195-
629 201, 2017.
630
631 **Hennings K, Arendt-Nielsen L, Andersen OK, 2005.** Orderly activation of human motor
632 neurons using electrical ramp prepulses. *Clin Neurophysiol,* 116:597-604, 2005.
633
634 **Hennings K, Arendt-Nielsen L, Andersen OK,** Breakdown of accommodation in nerve: a
635 possible role for persistent sodium current. *Theor Biol Med Model*., 2:16, 2005.
636
637 **Hilliges M, Wang L, Johansson O,** Ultrastructural evidence for nerve fibers within all vital
638 layers of the human epidermis. *J Invest Dermatol*., 104:134-137, 1995.
639

Hines LM, Carnevale NT, Hines Carnevale 1997 NEURON simulator environment. *Neural Comput*, 9:1179-1209, 1997.

Hovaguimian A, Gibbons CH, Diagnosis and treatment of pain in small-fiber neuropathy. *Curr Pain Headache Rep*., 15:193-200, 2011.

Hugosdottir R, Mørch CD, Andersen OK, Helgason T, Arendt-Nielsen L, Preferential activation of small cutaneous fibers through small pin electrode also depends on the shape of a long duration electrical current, *BMC Neuroscience*. 20:1-11, 2019

Inui K, Tran DT, Hoshiyama M, Kakigi, R, Preferential stimulation of Aδ fibers by intra-epidermal needle electrode in humans. *Pain* , 96:247–252, 2002.

Jankelowitz S, Howells J, Burke D, Plasticity of inwardly rectifying conductances following a corticospinal lesion in human subjects, *J Physiol*, Volume 581:927-940, 2007.

Kaube H, Katsarava Z, Käufer T, Diener H, Ellrich J. A new method to increase nociception specificity of the human blink reflex, *Clin Neurophysiol.*, 111:413-416, 2000.

Kiernan MC, Burke D, Andersen KV, Bostock H. Multiple measures of axonal excitability: A new approach in clinical testing, *Muscle & Nerve*, 23: 399-409, 2000.

Klein T1, Magerl W, Hopf HC, Sandkühler J, Treede RD, Perceptual Correlates of Nociceptive Long-Term Potentiation and Long-Term Depression in Humans. *The Journal of Neuroscience*, 24: 964 –971, 2004.

Kugelberg E, Accommodation in human nerves, *Acta Physiol Scand*, 8:1-115, 1944.

Lelic D, Mørch CD, Hennings K, Andersen OK, Drewes AM. Differences in perception and brain activation following stimulation by large versus small area cutaneous surface electrodes. *European journal of pain*, 16: 827-37, 2012.

Lucas K, On the rate of variation of the exciting current as a factor in electrical excitation, *J Physiol* **,** 36: 253-274, 1907.

Mørch CD, Henning K, Andersen O, Estimating nerve excitation thresholds to cutaneous electrical stimulation by finite element modeling combined with a stochastic branching nerve fiber model. *Medical and Biological Engineering and Computing*, 49: 385-395, 2011.

Myers IM, Peltier AC, Li J, Evaluating dermal myelinated nerve fibers in skin biopsy. *Muscle & Nerve*, 47:1–11, 2013.

Nilsson H, Schouenborg, J, Differential inhibitory effect on human nociceptive skin senses induced by local stimulation of thin cutaneous fibers. *Pain,* 80:103-112, 1999.

Motogi J, Sugiyama Y, Laakso I, Hirata A, Inui K, Tamura M, Muragaki Y. Selective Stimulation of C Fibers by an Intra-Epidermal Needle Electrode in Humans. The *Open Pain Journal*, 2:53-56, 2009.

689 **Poliak S, Salomon D, Elhanany H, Sabanay H, Kiernan B, Pevny L, Stewart CL, Xu**
690 **X, Chiu SY, Shrager P, Furley AJ, Peles E,** Juxtaparanodal clustering of Shaker-like K+
691 channels in myelinated axons depends on Caspr2 and TAG-1, *J Cell Biol.,* 162:1149-1160, ,
692 2003.
693
694 **Provitera V, Nolano M, Pagano A, Caporaso G, Stancanelli A, Santoro L,** Myelinated
695 nerve endings in human skin. *Muscle Nerve*, 35:767-75, 2007.
696
697 **Serra J, Bostock H, Solà R, Aleu J, García E, Cokic B, Navarro X, Quiles C,**
698 Microneurographic identification of spontaneous activity in C-nociceptors in neuropathic
699 pain states in humans and rats. *Pain*, 153:42-55, 2012.
700
701 **Serra J, Solà R, Aleu J, Quiles C, Navarro X, Bostock H,** Double and triple spikes in C-
702 nociceptors in neuropathic pain states: an additional peripheral mechanism of hyperalgesia.
703 *Pain,* 152:343-353, 2011.
704
705 **Smith MR, Smith RD, Plummer NW, Meisler MH, Goldin AL,** Functional Analysis of the
706 Mouse Scn8a Sodium Channel. *The Journal of Neuroscience*, 18: 6093–6102, 1998.
707
708 **Smith SM, Dworkin RH, Turk DC, Baron R, Polydefkis M, Tracey I, Borsook**
709 **D, Edwards RR, Harris RE, Wager TD, Arendt-Nielsen L, Burke LB, Carr**
710 **DB, Chappell A, Farrar JT, Freeman R, Gilron I, Goli V, Haeussler J, Jensen T, Katz**
711 **NP, Kent J, Kopecky EA, Lee DA, Maixner W, Markman JD, McArthur**
712 **JC, McDermott MP, Parvathenani L, Raja SN, Rappaport BA, Rice ASC, Rowbotham**
713 **MC, Tobias JK, Wasan AD, Witter J,** The Potential Role of Sensory Testing, Skin Biopsy,

and Functional Brain Imaging as Biomarkers in Chronic Pain Clinical Trials: IMMPACT Considerations. *J Pain*, 18: 757-777, 2017.

Sobanko J, Miller C, Alster T, Topical anesthetics for dermatologic procedures: a review. *Dermatol Surg*, 38:709-721, 2012.

Stoney SD, Machne X, Mechanisms of accommodation in different types of frog neurons, *J Gen Physiol.*, Issue 53: 248-262, 1969.

Tigerholm J, Petersson ME, Obreja O, Eberhardt E, Namer B, Weidner C, Lampert A, Carr RW, Schmelz M, Fransén E, C-fiber recovery cycle supernormality depends on ion concentration and ion channel permeability. *Biophys J*, 108:1057-71, 2015.

Tigerholm J1, Petersson ME, Obreja O, Lampert A, Carr R, Schmelz M, Fransén E. Modeling activity-dependent changes of axonal spike conduction in primary afferent C-nociceptors, *J Neurophysiol*., 111:1721-35, 2014.

van Hecke O, Austin SK, Khan RA, Smith BH, Torrance N, Neuropathic pain in the general population: a systematic review of epidemiological studies, *Pain,* 155: 654-662, 2014.

Watanabe S, Hoffman DA, Migliore M, Johnston D, Dendritic K+ channels contribute to spike-timing dependent long-term potentiation in hippocampal pyramidal neurons, *Proc Natl Acad Sci U S A*, 99:8366-8371, 2002.

Xia W, Mørch C, Andersen O, Test-Retest Reliability of 10 Hz Conditioning Electrical Stimulation Inducing Long-Term Potentiation (LTP)-Like Pain Amplification in Humans. *PLoS One*, 11, 2016.

Yawn BP1, Wollan PC, Weingarten TN, Watson JC, Hooten WM, Melton LJ 3rd, The prevalence of neuropathic pain: Clinical evaluation compared with screening tools in a community population. *Pain Med.*,10:586–593, 2009.

Figures

Figure 1. Study design. A. The definition of accommodation used in the current study. For long ramp pulses (> 20 ms), reduced excitability may occur, and the intensity needed for the subject to perceive the stimulus is increased (dashed line). B. The PTT technique. A surface electrode was placed on the skin, and the subject reported if the stimulus was perceived. The stimulus was a linear increased ramp current with the duration 1 ms, 10 ms, 25 ms, 50 ms, 100 ms and 200 ms. C. The computational model. The model consists of two nerve fiber models — one unmyelinated axon model representing the unmyelinated intraepidermal part of an Aδ fiber and one myelinated fiber model (Aβ) representing a large fiber. The extracellular potential was altered at the tip of the fibers to simulate the activation of nerves by the electrodes. The morphology of the Aβ model consists of three parts: node of Ranvier, juxtaparanode and internode. The figures are not drawn to scale.

*Figure 2. Accommodation of cutaneous nerves. The perception threshold for different duration of the ramp pulses for the pin electrode (A) and patch electrode (B.) C. Normalized perception threshold. The error bars represent the standard error. The asterisk represents statistically significant (*p <0.05) different perception thresholds.*

Figure 3. Voltage-gated ion channel currents during an action potential. The figures to the left represent an action potential generated in the $A\delta$ model and to the right the $A\beta$ model. The extracellular potential was altered for 1 ms with the shape of a ramp pulse. The onset of the stimulus occurred at time zero. A. Membrane potential. B. The small voltage-gated ion channel currents. C. The large voltage-gated ion channel currents. The current density for the potassium current was low for the K_{Dr} current ($A\beta$ model) since the combined area of the juxtaparanode was 3.33 times larger than the node of Ranvier.

Figure 4. Accommodation generated by the computational model. A. The extracellular potential alteration needed to generate an action potential which propagates to the end of the nerve fiber model. B. The extracellular potential normalized to the 1 ms duration of the stimulus. The generation of an action potential for different durations of the ramp stimulation for the $A\delta$ model (C) and $A\beta$ model (D). The membrane potential for $A\delta$ (E) and $A\beta$ model (F) when the extracellular potential alteration was increased from 10 mV to 30 mV (duration=200 ms). The onset of the stimulus occurred at time zero.

Figure 5. The influence of the maximum conductance on activation threshold. All currents were increased by 30 %. For the larger currents, spiking sodium and delayed rectifier, the maximum conductance was altered by 10% and 20% respectively. The green dotted line in figure B represents the normalized extracellular potential when the maximum conductance of both the K_M and delayed rectifier (K_{Dr}) currents was reduced by 50%.

Figure 6. The influence of voltage-gated ion channels on accommodation. To study the influence of specific different ion channels, either the conductances were altered, or the ion channel was removed from the model. The maximum conductance of the K_{Dr} was varied in

the two nerve fiber models (blue lines). All slow currents (K_M, Na_P, and HCN) were removed from the models (light blue line), and all the ion channels were removed from the model except the Na_{TTXs} for $A\beta$ model and Na_{TTXr} for the $A\delta$ model (light blue lines). To compensate for the high excitability, the conductance of the sodium channels was reduced by 54% for the case when all the ion channels were removed except for the spiking sodium channel. Note that accommodation could be generated in the $A\beta$ model when the model only Na_{TTXs} channel was implemented (light blue lines).

Figure 7. The influence of Inactivation of sodium channels. A. The membrane potential generated by a 10 mV ramp stimulation alteration of the extracellular potential (duration=200 ms). B. The total inactivation of the sodium channels (Na_{TTXs} or Na_{TTXr}) for all of the inactivation gates. C-F. The onset of the stimulus occurred at time zero. All the steady-state inactivation curves of either the Na_{TTXs} ($A\beta$ model) or Na_{TTXr} ($A\delta$ model) were shifted, and the accommodation recalculated. A negative shift is defined as a hyperpolarized shift of all of the steady-state inactivation curves and a positive shift as a depolarizing shift. To compensate for the general excitability, the maximum conductance of the Na_{TTXs} was increased ($A\beta$ model) or the Na_{TTXr} altered ($A\delta$ model) to retain a similar activation threshold (within 5%) for 1 ms ramp as in the control model (no shifts of the steady-state inactivation curves).

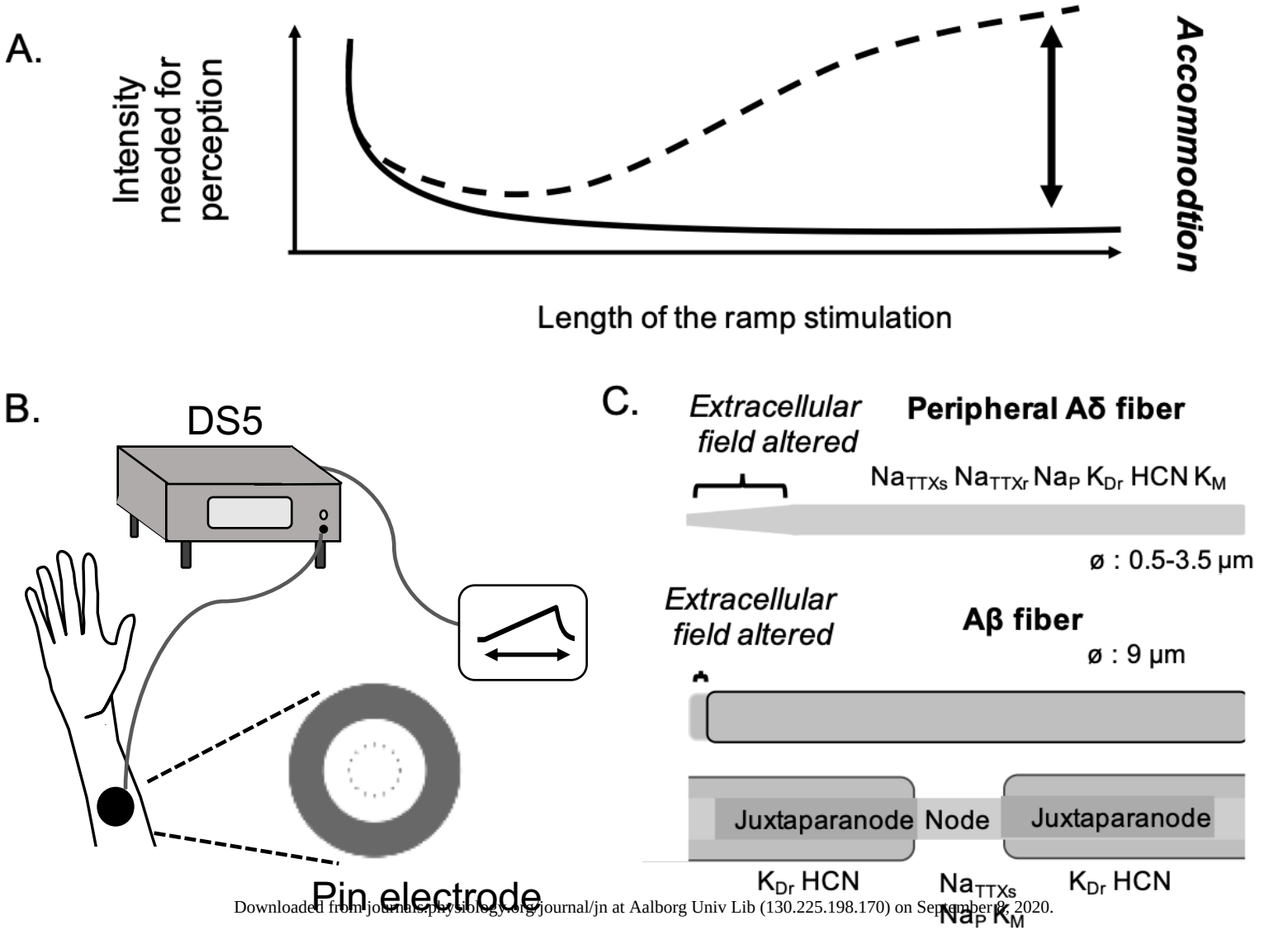

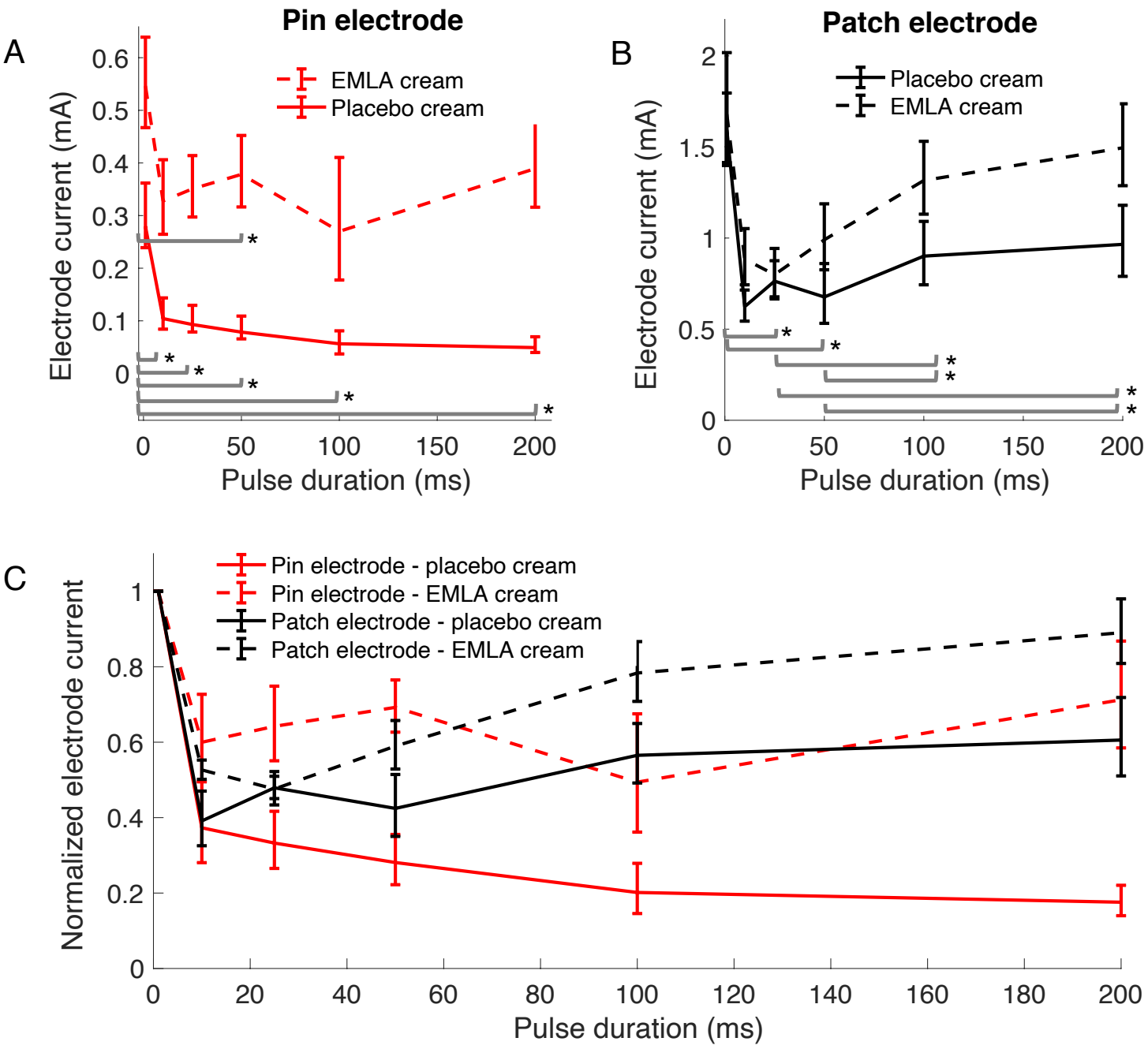

A

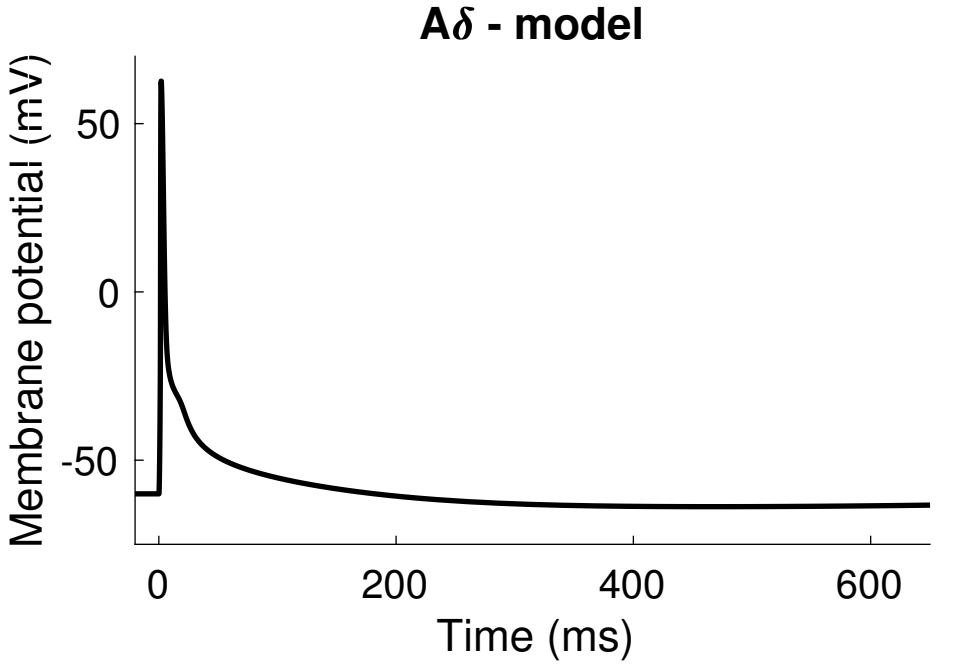

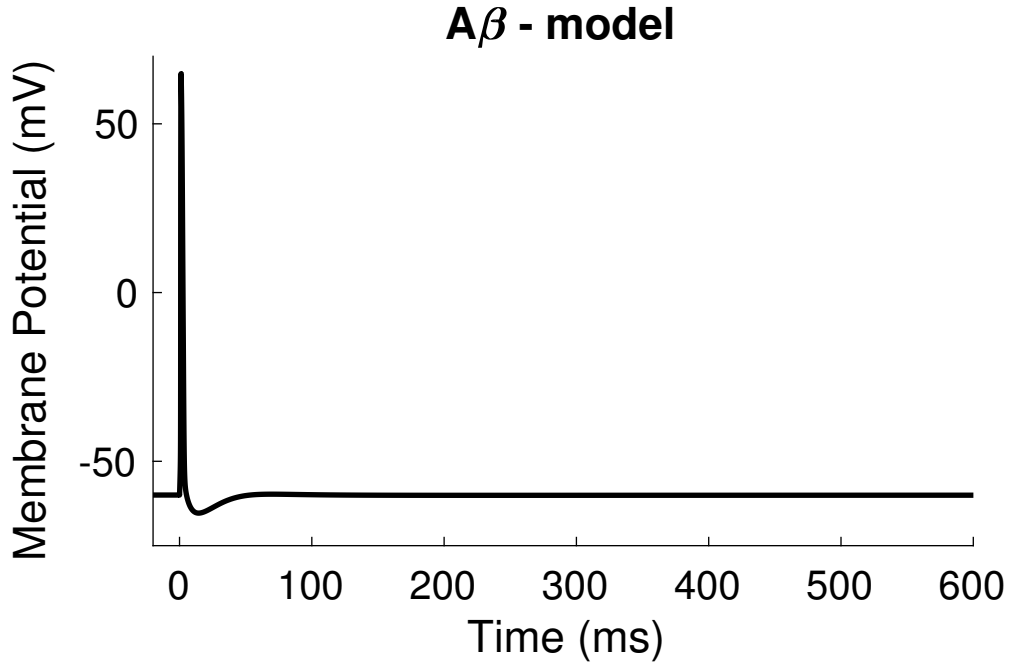

B

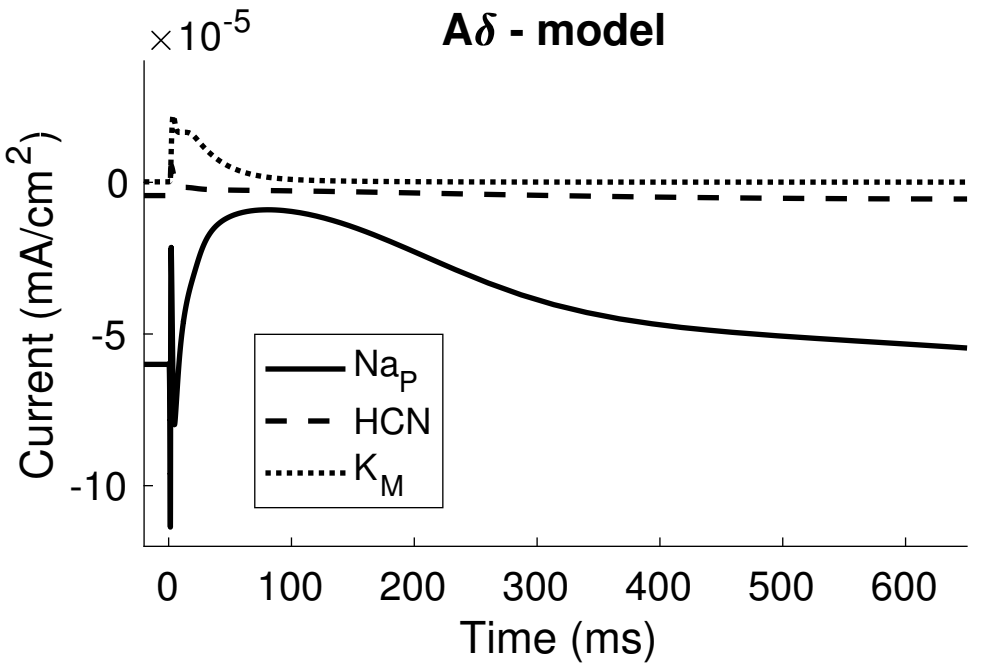

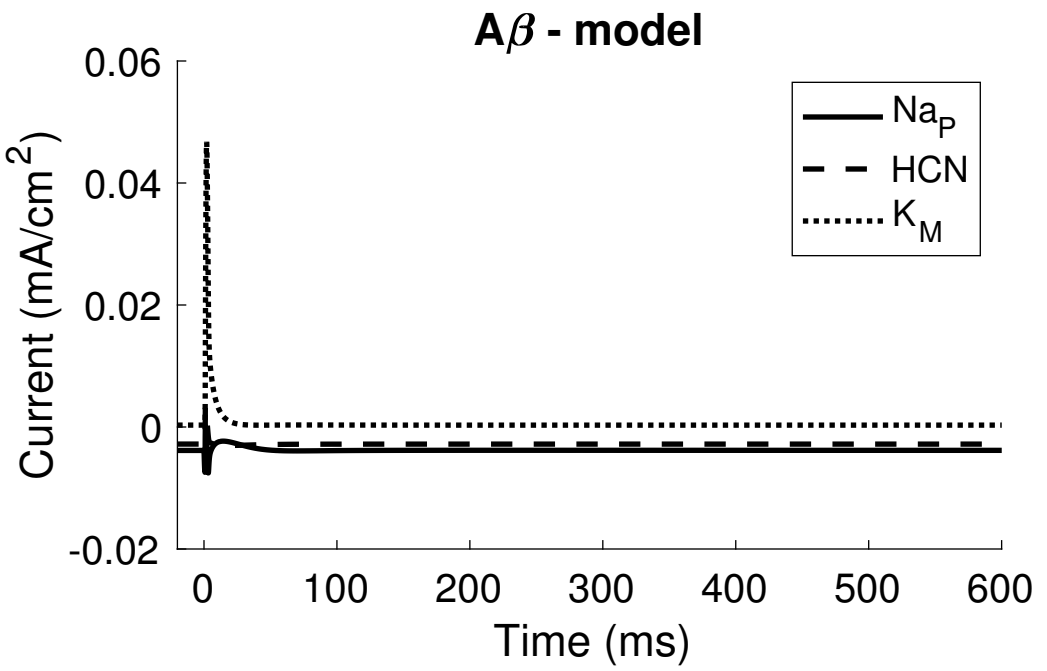

C